Inorg. Chem. **2007**, *46*, 5567–5575

A New N,N,O Chelate for Transition Metal Chemistry: Fe_5 and Fe_6 Clusters from the Use of 6-Hydroxymethyl-2,2′-bipyridine (hmbpH)

Rashmi Bagai, Khalil A. Abboud, and George Christou*

Department of Chemistry, University of Florida, Gainesville, Florida 32611-7200

Received January 30, 2007

The initial use of the anion of 6-hydroxymethyl-2,2′-bipyridine (hmbpH) as a chelate in coordination chemistry is described. The syntheses, crystal structures, and magnetochemical characterization are reported of four new iron(III) clusters $[Fe_5O_2(OH)(O_2CMe)_5(hmbp)_3](ClO_4)_2$ (**1**) and $[Fe_6O_2(OH)_2(O_2CR)_6(hmbp)_4](NO_3)_2$ (R = Ph (**2**), Me (**3**), Bu^t (**4**); hmbpH = 6-hydroxymethyl-2,2′-bipyridine). The reaction of $Fe(ClO_4)_3$, hmbpH, and sodium acetate in a 1:1:∼4 ratio in EtOH gave **1**, and the reaction between $[Fe_3O(O_2CR)_6(H_2O)_3](NO_3)$ (R = Ph, Me, Bu^t) and hmbpH in a 1:1 ratio in MeCN gave **2**–**4**, respectively. The core of **1** consists of a $[Fe_4(\mu_3\text{-}O)_2]^{8+}$ butterfly unit to which is attached a fifth Fe atom by bridging O atoms. The core of **2**–**4** also consists of a $[Fe_4(\mu_3\text{-}O)_2]^{8+}$ butterfly unit to which are attached an Fe atom on either side by bridging O atoms. Variable-temperature (*T*) and -field (*H*) solid-state DC and AC magnetization (*M*) studies were carried out on complexes **1**–**4** in the 5.0–300 K range. Fitting of the data revealed that **1** has an $S = 5/2$ ground state spin whereas **2**–**4** possess an $S = 5$ ground state. Fitting of the $M/N\mu_B$ vs H/T data by matrix diagonalization and including only axial zero-field splitting (ZFS) gave values of the axial ZFS parameter $|D|$ of 0.75, 0.36, 0.46, and 0.36 cm^{-1} for **1**–**4,** respectively.

Introduction

There continues to be a great interest by many groups around the world in the synthesis and study of 3d transition metal cluster compounds, not least for the structural aesthetics possessed by such species. Other reasons for this interest are varied. For iron(III) chemistry, for example, there are bioinorganic areas of relevance such as the great desire to understand and model the assembly of the polynuclear iron core of the iron storage protein ferritin.[1−3] There is also a materials interest in that high-nuclearity iron compounds can sometimes exhibit unusual and occasionally novel magnetic properties, with some of them even being examples of single-molecule magnets (SMMs);[4−6] the latter are molecules with a combination of a relatively large ground state spin and a significant magnetoanisotropy of the easy-axis (Ising) type.[6,7] That Fe(III) is one area where high-nuclearity species are often encountered is as expected from the high charge-to-size ratio of this oxidation state and the resulting propensity to favor oxide-bridged multinuclear products. Indeed, the formation of the Fe/O/OH core of ferritin that was mentioned as a bioinorganic area of interest is merely an extreme example of such polynuclear chemistry. As a result, many large Fe(III) clusters have been reported to date with nuclearities up to 22.[8−15]

Although the exchange interactions between Fe(III) centers are almost always antiferromagnetic, certain Fe_x topologies can nevertheless possess large ground-state spin values as a

* To whom correspondence should be addressed. Tel: +1-352-392-8314. Fax: +1-352-392-8757. E-mail: christou@chem.ufl.edu.

(1) Bertini, I.; Gray, H. B.; Lippard, S. J.; Valentine, J. S. *Bioinorganic Chemistry*; University Science Books: Mill Valley, CA, 1994; p 611.
(2) Taft, K. L.; Papaefthymiou, G. C.; Lippard, S. J. *Science* **1993**, *259*, 1302−1305.
(3) Gorun, S. M.; Papaefthymiou, G. C.; Frankel, R. B.; Lippard, S. J. *J. Am. Chem. Soc.* **1987**, *109*, 3337−3348.
(4) Sangregorio, C.; Ohm, T.; Paulsen, C.; Sessoli, R.; Gatteschi, D. *Phys. Rev. Lett.* **1997**, *78*, 4645−4648.
(5) Christou, G.; Gatteschi, D.; Hendrickson, D. N.; Sessoli, R. *MRS Bull.* **2000**, *25*, 66−71.
(6) Gatteschi, D.; Sessoli, R.; Cornia, A. *Chem. Commun.* **2000**, 725−732.
(7) Oshio, H.; Hoshino, N.; Ito, T.; Nakano, M. *J. Am. Chem. Soc.* **2004**, *126*, 8805−8812.
(8) Powell, A. K.; Heath, S. L.; Gatteschi, D.; Pardi, L.; Sessoli, R.; Spina, G.; Del Giallo, F.; Pieralli, F. *J. Am. Chem. Soc.* **1995**, *117*, 2491−502.
(9) Goodwin, J. C.; Sessoli, R.; Gatteschi, D.; Wernsdorfer, W.; Powell, A. K.; Heath, S. L. *Dalton* **2000**, 1835−1840.
(10) Foguet-Albiol, D.; Abboud, K. A.; Christou, G. *Chem. Commun.* **2005**, 4282−4284.
(11) Benelli, C.; Parsons, S.; Solan, G. A.; Winpenny, R. E. P. *Angew. Chem., Int. Ed.* **1996**, *35*, 1825−1828.
(12) Benelli, C.; Cano, J.; Journaux, Y.; Sessoli, R.; Solan, G. A.; Winpenny, R. E. P. *Inorg. Chem.* **2001**, *40*, 188−189.
(13) Powell, G. W.; Lancashire, H. N.; Brechin, E. K.; Collison, D.; Health, S. L.; Malluh, T.; Wernsdorfer, W. *Angew. Chem., Int. Ed.* **2004**, *43*, 5772−5775.

10.1021/ic070174i CCC: $37.00
Published on Web 06/05/2007

Scheme 1

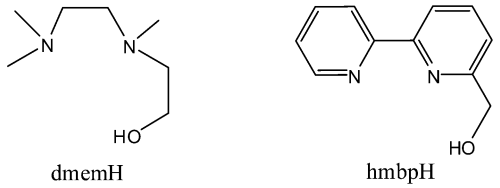

result of spin frustration. The latter is here defined in its more general sense of competing exchange interactions of comparable magnitude, preventing (frustrating) the preferred antiparallel alignment of all spins, and thus giving larger ground state spin values than might be expected.[8,10,16−21] In some cases, as mentioned above, the compounds can behave as SMMs. This is the case for clusters such as $[Fe_8O_2(OH)_{12}(tacn)_6]^{8+}$ [4,22,23] and $[Fe_4(OMe)_6(dpm)_6]$[24] for example.

For the above reasons and more, there is a continuing search for new synthetic methods that can yield new polynuclear Fe/O clusters. One approach that has proven successful in this regard is the use of alcohol-containing chelate groups that, on deprotonation, can provide alkoxide groups that are excellent bridging units and thus foster formation of high nuclearity products.[19,25−27] We recently reported, for example, the use of deprotonated dmemH as a new and flexible N,N,O chelate for the synthesis of Fe_3, Fe_6, and two Fe_7 complexes (Scheme 1), some of which possess novel Fe_x topologies. As part of these continuing efforts to synthesize new Fe_x clusters, we have now turned to another potential chelating group that has also never before been employed, to our knowledge, in transition metal chemistry. This is 6-hydroxymethyl-2,2′-bipyridine (hmbpH; Scheme 1), whose deprotonated form, like $dmem^-$, would be a potential N,N,O chelate, but a more rigid one than $dmem^-$.

Scheme 2[a]

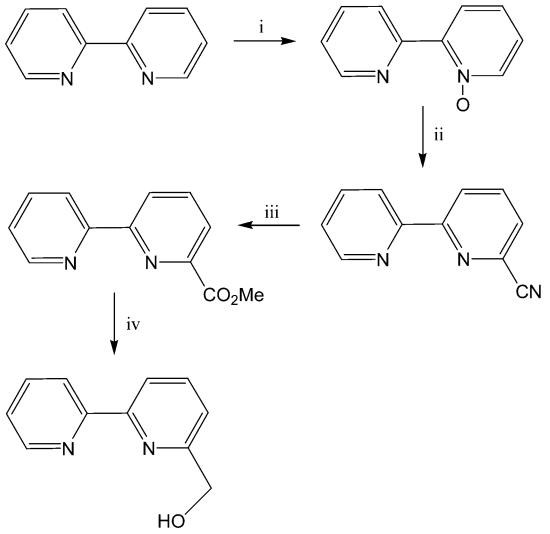

[a] (i) H_2O_2, CF_3CO_2H (ref 36) (ii) Me_3SiCN, PhCOCl, CH_2Cl_2 (ref 37) (iii) NaOMe, MeOH (ref 37) (iv) (a) $NaBH_4$, EtOH(b) H_2SO_4, H_2O (ref 38)

In fact, hmbpH was selected as a "fusion" of two chelates that have each proven a rich source of M_x, and particularly Fe_x, species in the past, 2,2′-bipyridine and the anion of 2-(hydroxymethyl)pyridine (hmpH).[17,28−34] We thus considered it a potentially viable route to new clusters and probably of a different type than previously encountered with bpy or hmp^- separately. Our first investigations with hmbpH have been in Fe(III) chemistry, and we have indeed found it to lead to new structural types of products. We herein report the first results from this study, the syntheses, crystal structures, and magnetochemical characterization of new Fe_5 and Fe_6 molecular species.

Experimental Section

Syntheses. All preparations were performed under aerobic conditions using reagents and solvents as received. $[Fe_3O(O_2CBu^t)_6(H_2O)_3](NO_3)$, $[Fe_3O(O_2CPh)_6(H_2O)_3](NO_3)$, and $[Fe_3O(O_2CMe)_6(H_2O)_3](NO_3)$ were synthesized as reported elsewhere.[35] The known organic molecule hmbpH was synthesized, according to Scheme 2, using previously reported procedures.[36−38]

$[Fe_5O_2(OH)(O_2CMe)_5(hmbp)_3](ClO_4)_2$ (1). To a stirred solution of $Fe(ClO_4)_3 \cdot xH_2O$ (0.19 g, 0.54 mmol) and sodium acetate (0.18

(14) Murugesu, M.; Clerac, R.; Wernsdorfer, W.; Anson, C. E.; Powell, A. K. *Angew. Chem., Int. Ed.* **2005**, *44*, 6678−6682.
(15) Ammala, P.; Cashion, J. D.; Kepert, C. M.; Moubaraki, B.; Murray, K. S.; Spiccia, L.; West, B. O. *Angew. Chem., Int. Ed.* **2000**, *39*, 1688−1690.
(16) Canada-Vilalta, C.; O'Brien Ted, A.; Brechin Euan, K.; Pink, M.; Davidson Ernest, R.; Christou, G. *Inorg. Chem.* **2004**, *43*, 5505−5521.
(17) McCusker, J. K.; Vincent, J. B.; Schmitt, E. A.; Mino, M. L.; Shin, K.; Coggin, D. K.; Hagen, P. M.; Huffman, J. C.; Christou, G.; Hendrickson, D. N. *J. Am. Chem. Soc.* **1991**, *113*, 3012−3021.
(18) Murugesu, M.; Abboud, K. A.; Christou, G. *Dalton Trans.* **2003**, 4552−4556.
(19) Jones, L. F.; Brechin, E. K.; Collison, D.; Helliwell, M.; Mallah, T.; Piligkos, S.; Rajaraman, G.; Wernsdorfer, W. *Inorg. Chem.* **2003**, *42*, 6601−6603.
(20) Kahn, O. *Chem. Phys. Lett.* **1997**, *265*, 109−114.
(21) McCusker, J. K.; Christmas, C. A.; Hagen, P. M.; Chadha, R. K.; Harvey, D. F.; Hendrickson, D. N. *J. Am. Chem. Soc.* **1991**, *113*, 6114−6124.
(22) Delfs, C.; Gatteschi, D.; Pardi, L.; Sessoli, R.; Wieghardt, K.; Hanke, D. *Inorg. Chem.* **1993**, *32*, 3099−3103.
(23) Barra, A. L.; Gatteschi, D.; Sessoli, R. *Chem. Eur. J.* **2000**, *6*, 1608−1614.
(24) Barra, A. L.; Caneschi, A.; Cornia, A.; de Biani, F. F.; Gatteschi, D.; Sangregorio, C.; Sessoli, R.; Sorace, L. *J. Am. Chem. Soc.* **1999**, *121*, 5302−5310.
(25) Jones, L. F.; Batsanov, A.; Brechin, E. K.; Collison, D.; Helliwell, M.; Mallah, T.; McInnes, E. J. L.; Piligkos, S. *Angew. Chem., Int. Ed.* **2002**, *41*, 4318−4321.
(26) Moragues-Canovas, M.; Riviere, E.; Ricard, L.; Paulsen, C.; Wernsdorfer, W.; Rajaraman, G.; Brechin, E. K.; Mallah, T. *Adv. Mater.* **2004**, *16*, 1101−1105.
(27) Saalfrank, R. W.; Bernt, I.; Uller, E.; Hampel, F. *Angew. Chem., Int. Ed.* **1997**, *36*, 2482−2485.
(28) Bacsa, J.; Zhao, H.; Dunbar, K. R. *Acta Crystallogr., Sect. C: Cryst. Struct. Commun.* **2003**, *C59*, m561−m564.
(29) Canada-Vilalta, C.; O'Brien Ted, A.; Pink, M.; Davidson, Ernest, R.; Christou, G. *Inorg. Chem.* **2003**, *42*, 7819−7829.
(30) Wemple, M. W.; Coggin, D. K.; Vincent, J. B.; McCusker, J. K.; Strieb, W. E.; Huffman, J. C.; Hendrickson, D. N.; Christou, G. *J. Chem. Soc., Dalton Trans.* **1998**, 719−725.
(31) Yan, B.; Chen, Z. D. *Inorg. Chem. Commun.* **2001**, *4*, 138−141.
(32) Seddon, E. J.; Huffman, J. C.; Christou, G. *Dalton* **2000**, 4446−4452.
(33) Brechin, E. K.; Knapp, M. J.; Huffman, J. C.; Hendrickson, D. N.; Christou, G. *Inorg. Chim. Acta* **2000**, *297*, 389−399.
(34) Christmas, C. A.; Tsai, H. L.; Pardi, L.; Kesselman, J. M.; Gantzel, P. K.; Chadha, R. K.; Gatteschi, D.; Harvey, D. F.; Hendrickson, D. N. *J. Am. Chem. Soc.* **1993**, *115*, 12483−12490.
(35) Bond, A. M.; Clark, R. J. H.; Humphrey, D. G.; Panayiotopoulos, P.; Skelton, B. W.; White, A. H. *J. Chem. Soc., Dalton Trans.* **1998**, 1845−1852 and references therein.
(36) Demnitz, F. W. J.; D'Heni, M. B. *Org. Prep. Proc. Int.* **1998**, *30*, 467−469.
(37) Heirtzler, F. R. *Synlett* **1999**, *8*, 1203−1206.
(38) Norrby, T.; Borje, A.; Zhang, L.; Akermark, B. *Acta Chem. Scand.* **1998**, *52*, 77−85.

Table 1. Crystallographic Data for **1**·5MeCN and **2**·3MeCN·H_2O

	1	**2**
formula[a]	$C_{53}H_{58}Cl_2Fe_5N_{11}O_{24}$	$C_{92}H_{79}Fe_6N_{13}O_{27}$
fw, g/mol[a]	1583.25	2133.77
space group	$P2_1/c$	$P\bar{1}$
a, Å	21.6352(2)	13.8233(6)
b, Å	13.4154(6)	14.0671(6)
c, Å	23.1971(11)	14.2856(6)
α, °	90	65.175(2)
β, °	102.456(2)	70.147(2)
γ, °	90	89.561(2)
V, Å^3	6574.4(5)	2341.55(17)
Z	4	1
T, K	173(2)	173(2)
radiation, Å[b]	0.71073	0.71073
ρ_{calc}, g/cm^3	1.600	1.512
μ, mm^{-1}	1.244	0.990
R1[c,d]	0.0611	0.0487
wR2[e]	0.1705	0.1276

[a] Including solvate molecules. [b] Graphite monochromator. [c] $I > 2\sigma(I)$. [d] $R1 = \sum(||F_o| - |F_c||)/\sum|F_o|$. [e] $wR2 = [\sum[w(F_o^2 - F_c^2)^2]/\sum[w(F_o^2)^2]]^{1/2}$, $w = 1/[\sigma^2(F_o^2) + [(ap)^2 + bp]$, where $p = [\max(F_o^2, O) + 2F_c^2]/3$.

g, 2.0 mmol) in EtOH (15 mL) was added hmbpH (0.10 g, 0.54 mmol). The resulting orange solution was stirred for 3 h at room temperature, during which time precipitated an orange solid. The precipitate was collected by filtration, washed with EtOH, and dried. It was then dissolved in MeCN (15 mL), filtered, and the filtrate layered with Et_2O. X-ray quality crystals of **1**·5MeCN slowly grew over 5 days in 18% yield. These were collected by filtration, washed with MeCN, and dried in vacuo; dried solid analyzed as solvent-free. Anal. Calcd (Found) for **1** ($C_{43}H_{43}N_6Cl_2Fe_5O_{24}$): C, 37.48 (37.05); H, 3.14 (3.12); N, 6.09 (5.89). Selected IR data (cm^{-1}): 1599(s), 15429s), 1490(m), 1402(s), 1175(m), 1068(m), 1025(m), 937(w), 820(w), 777(m), 719(s), 663(s), 600(w), 547(w), 463(m).

$[Fe_6O_2(OH)_2(O_2CPh)_6(hmbp)_4](NO_3)_2$ (2). An orange-red solution of $[Fe_3O(O_2CPh)_6(H_2O)_3](NO_3)$ (0.14 g, 0.14 mmol) in MeCN (20 mL) was treated with hmbpH (0.05 g, 0.27 mmol). The solution was stirred for 2 h and filtered, and the orange-red filtrate left undisturbed to concentrate slowly by evaporation. X-ray quality, orange-red crystals of **2**·3MeCN·H_2O formed over 5 days in 25% yield. These were collected by filtration, washed with MeCN and dried in vacuo. Anal. Calcd (Found) for **2**·H_2O ($C_{86}H_{70}N_{10}Fe_6O_{27}$): C, 51.37 (51.34); H, 3.51 (3.37); N, 6.97 (6.82). Selected IR data (cm^{-1}): 3426(br), 1602(m), 1539(s), 1490(m), 1433(s), 1350(m), 1299(w), 1254(w), 1226(w), 1088(s), 1044(s), 779(m), 690(m), 662(m), 623(m), 556(m), 429(w).

$[Fe_6O_2(OH)_2(O_2CMe)_6(hmbp)_4](NO_3)_2$ (3). An orange-red solution of $[Fe_3O(O_2CMe)_6(H_2O)_3](NO_3)$ (0.11 g, 0.17 mmol) in MeCN (20 mL) was treated with hmbpH (0.065 g, 0.35 mmol). The solution was stirred for 2 h and filtered, and the orange-red filtrate left undisturbed to concentrate slowly by evaporation. Orange-red crystals formed over 5 days in 15% yield. These were collected by filtration, washed with MeCN, and dried in vacuo. Anal. Calcd (Found) for **3**·H_2O ($C_{56}H_{58}N_{10}Fe_6O_{27}$): C, 41.06 (41.13); H, 3.57 (3.61); N, 8.55 (8.33). Selected IR data (cm^{-1}): 3399(br), 1601(m), 1546(s), 1491(m), 1438(s), 1384(s), 1256(w), 1225(w), 1166(w), 1090(w), 1037(s), 905(w), 833(w), 781(m), 664(s), 645(m), 556(m), 434(w), 413(w).

$[Fe_6O_2(OH)_2(O_2CBu^t)_6(hmbp)_4](NO_3)_2$ (4). An orange-red solution of $[Fe_3O(O_2CBu^t)_6(H_2O)_3](NO_3)$ (0.13 g, 0.14 mmol) in MeCN (20 mL) was treated with hmbpH (0.05 g, 0.27 mmol). The solution was stirred for 2 h and filtered, and the orange-red filtrate layered with Et_2O. Orange crystals slowly grew over 4 days in 20% yield. Anal. Calcd (Found) for **4**·H_2O ($C_{74}H_{94}N_{10}Fe_6O_{27}$): C, 47.01 (46.64); H, 5.01 (4.76); N, 7.41 (7.50). Selected IR data (cm^{-1}): 3408(br), 3077(w), 2962(m), 1601(w), 1539(s), 1484(m), 1459(m), 1425(s), 1383(s), 1361(s), 1300(w), 1227(m), 1163(w), 1091(w), 1036(m), 900(w), 832(w), 785(m), 663(s), 600(m), 553(m), 434(m).

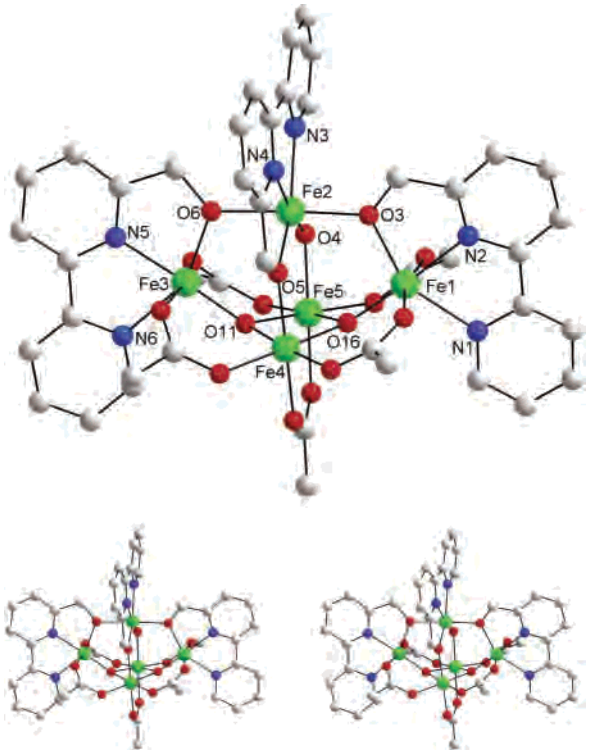

Figure 1. Labeled representation of the structure of **1**. Hydrogen atoms have been omitted for clarity. Color code: Fe^{III}, green; O, red; N, blue; C, gray.

Table 2. Selected Bond Distances (Å) and Angles (deg) for **1**·5MeCN

Fe1−O16	1.825(3)	Fe3−O7	2.048(3)
Fe1−O3	2.021(3)	Fe5−O13	2.041(3)
Fe1−O15	2.058(3)	Fe3−O9	2.063(3)
Fe1−O1	2.075(3)	Fe3−N5	2.094(4)
Fe1−N2	2.104(3)	Fe3−N6	2.189(4)
Fe1−N1	2.190(3)	Fe4−O16	1.951(3)
Fe2−O4	1.933(3)	Fe4−O11	1.956(3)
Fe2−O5	1.980(3)	Fe4−O14	2.003(3)
Fe2−O3	2.023(3)	Fe4−O10	2.017(3)
Fe2−O6	2.052(3)	Fe4−O12	2.039(3)
Fe2−N4	2.116(4)	Fe4−O5	2.058(3)
Fe2−N3	2.155(5)	Fe5−O11	1.951(3)
Fe3−O11	1.826(3)	Fe5−O16	1.951(3)
Fe3−O6	2.008(3)	Fe5−O2	2.017(3)
Fe5−O8	2.021(3)	Fe5−O4	2.031(3)
Fe1−O16−Fe4	129.68(14)	Fe2−O5−Fe4	118.09(14)
Fe1−O3−Fe2	114.99(14)	Fe4−O16−Fe5	94.61(11)
Fe2−O4−Fe5	119.95(15)	Fe5−O11−Fe4	94.45(11)
Fe1−O16−Fe5	126.63(14)	Fe3−O11−Fe5	125.89(15)
Fe3−O6−Fe2	112.45(14)		

X-ray Crystallography. Data were collected on a Siemens SMART PLATFORM equipped with a CCD area detector and a graphite monochromator utilizing Mo K_α radiation ($\lambda = 0.71073$ Å). Suitable crystals of **1**·5MeCN and **2**·3MeCN·H_2O were attached to glass fibers using silicone grease and transferred to a goniostat where they were cooled to 173 K for data collection. Cell parameters were refined using up to 8192 reflections. A full sphere of data (1850 frames) was collected using the ω-scan method (0.3° frame width). The first 50 frames were remeasured at the end of the data collection to monitor instrument and crystal stability (maximum

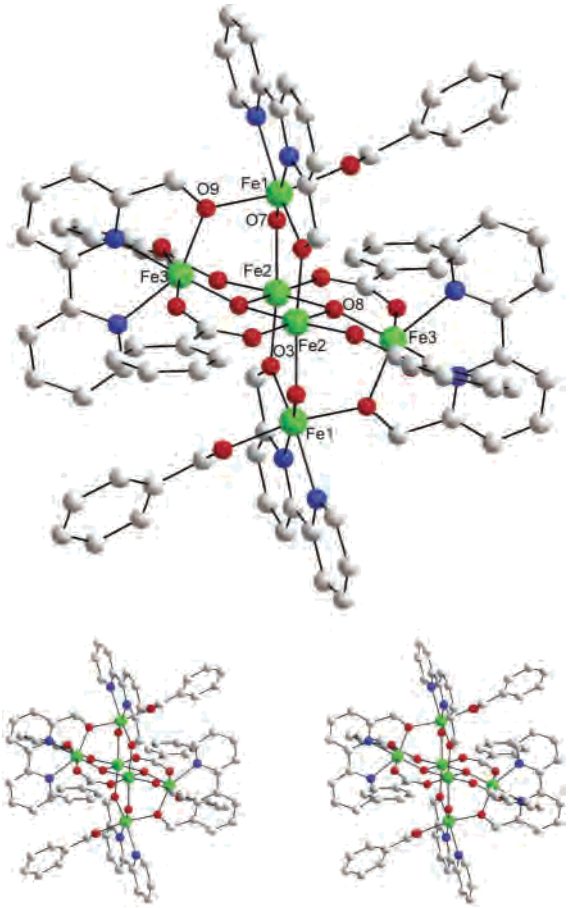

Figure 2. Labeled representation of the structure of **2**. Hydrogen atoms have been omitted for clarity. Color code: Fe^{III}, green; O, red; C, gray; N, blue.

correction on I was <1%). Absorption corrections by integration were applied based on measured indexed crystal faces. The structure was solved by the direct methods in *SHELXTL6*, and refined on F^2 using full-matrix least-squares. The non-H atoms were treated anisotropically, whereas the hydrogen atoms were calculated in ideal positions and refined as riding on their respective carbon atoms.

In **1**·5MeCN, the asymmetric unit consists of the Fe_5 cluster, two ClO_4^- anions, and five MeCN solvent molecules. The latter molecules were disordered and could not be modeled properly; thus, the program SQUEEZE,[39] a part of the PLATON package of crystallographic software, was used to calculate the solvent disorder area and remove its contribution to the overall intensity data. One of the ClO_4^- anions was disordered and was refined in two positions with their site occupation factors refined dependently. Both disorder components are H-bonded to the hydroxyl proton on O4. A total of 720 parameters were refined in the final cycle of refinement using 42 942 reflections with $I > 2\sigma(I)$ to yield R1 and wR2 of 6.11% and 17.05%, respectively.

In **2**·3MeCN·H_2O, the asymmetric unit consists of a half Fe_6 cluster, one and a half MeCN molecules, one NO_3^- anion disordered over three positions, and a half water molecule which exists counter to one of the half NO_3^- anions. One nitrate exists with 50% occupancy, while the other has all but one O atom disordered. The latter was refined in two parts with occupation factors fixed at 20% and 30%. A total of 633 parameters were refined in the final cycle of refinement using 15 661 reflections with $I > 2\sigma(I)$ to yield R1 and wR2 of 4.85% and 12.76%, respectively.

Table 3. Selected Bond Distances (Å) and Angles (deg) for **2**·3MeCN·H_2O

Fe1−O7′	1.912(2)	Fe2−O5	2.029(2)
Fe1−O3	1.974(2)	Fe2−O4	2.033(2)
Fe1−O9′	2.046(2)	Fe2−O3	2.063(2)
Fe1−O1	2.059(2)	Fe3−O8	1.832(2)
Fe1−N2	2.097(3)	Fe3−O9	2.015(2)
Fe1−N1	2.186(3)	Fe3−O6	2.031(2)
Fe2−O8	1.938(2)	Fe3−O10	2.049(2)
Fe2−O8′	1.978(2)	Fe3−N3	2.095(3)
Fe2−O7	2.011(2)	Fe3−N4	2.183(3)
Fe1−O3−Fe2	120.78(10)	Fe1′−O7−Fe2	125.85(11)
Fe3−O8−Fe2′	129.12(11)	Fe3−O9−Fe1′	116.32(10)

Unit cell data and structure refinement details for the two compounds are listed in Table 1.

Other Studies. Infrared spectra were recorded in the solid state (KBr pellets) on a Nicolet Nexus 670 FTIR spectrometer in the 400−4000 cm^{-1} range. Elemental analyses (C, H, N) were performed by the in-house facilities of the University of Florida, Chemistry Department. Variable-temperature DC and AC magnetic susceptibility data were collected at the University of Florida using a Quantum Design MPMS-XL SQUID susceptometer equipped with a 7 T magnet and operating in the 1.8−300 K range. Samples were embedded in solid eicosane to prevent torquing. Magnetization vs field and temperature data were fit using the program MAGNET. Pascal's constants[40] were used to estimate the diamagnetic correction, which was subtracted from the experimental susceptibility to give the molar paramagnetic susceptibility (χ_M).

Results and Discussion

Syntheses. The reaction of $Fe(ClO_4)_3$ with hmbpH and sodium acetate in a 1:1:4 ratio in EtOH gave an orange precipitate that after recrystallization from MeCN/Et_2O gave crystals of the novel pentanuclear cluster **1**. The acetate acts as the proton acceptor in this reaction, as well as providing ligand groups. The same product was also obtained using MeCN as the reaction solvent, but the precipitate was found to be contaminated with some other solid products. The formation of **1** is summarized in eq 1.

$$5Fe^{3+} + 3\text{hmbpH} + 13MeCO_2^- + 3H_2O \rightarrow [Fe_5O_2(OH)(O_2CMe)_5(\text{hmbp})_3]^{2+} + 8MeCO_2H \quad (1)$$

Decreasing the amount of acetate from 4 to 2 equiv reduces the reaction yield, as expected from eq 1. Other reactions with small variations in the Fe^{3+}/hmbpH/$MeCO_2^-$ ratio also gave compound **1**.

Many synthetic procedures to polynuclear iron clusters rely on the reaction of $[Fe_3O(O_2CR)_6L_3]^+$ species with a potentially chelating ligand,[11,18,33,34,41−43] and we thus also explored this starting material for reactions with hmbpH. In such reactions, the $[Fe_3O]^{7+}$ core of the trinuclear iron complex serves as a useful building block for higher-nuclearity

(39) Van der Sluis, P.; Spek, A. L. *Acta Crystallogr., Sect. A: Found. Crystallogr.* **1990**, *A46*, 194−201.

(40) Weast, R. C., Ed. *CRC Handbook of Chemistry and Physics*, 64th ed.; CRC Press: Cleveland, 1984; p 2320.

(41) Tolis, E. I.; Helliwell, M.; Langley, S.; Raftery, J.; Winpenny, R. E. P. *Angew. Chem., Int. Ed.* **2003**, *42*, 3804−3808.

(42) Murugesu, M.; Abboud, K. A.; Christou, G. *Polyhedron* **2004**, *23*, 2779−2788.

(43) Taft, K. L.; Lippard, S. J. *J. Am. Chem. Soc.* **1990**, *112*, 9629−9630.

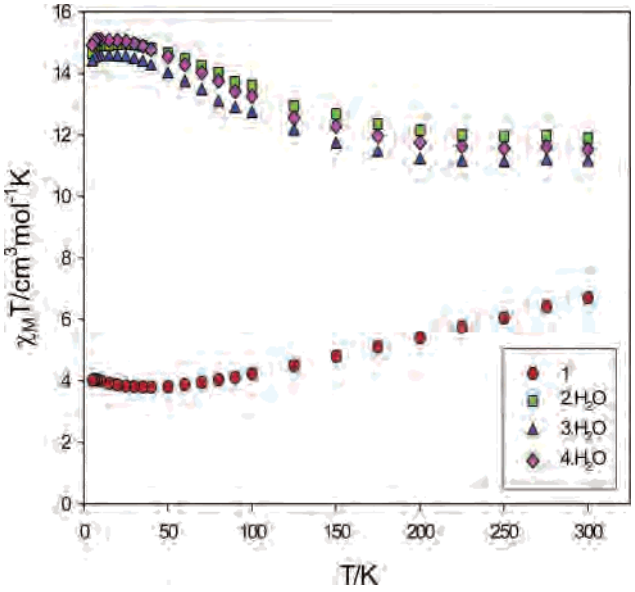

Figure 3. Plots of $\chi_M T$ vs T for complexes **1** (●), **2** (■), **3** (▲), and **4** (◆).

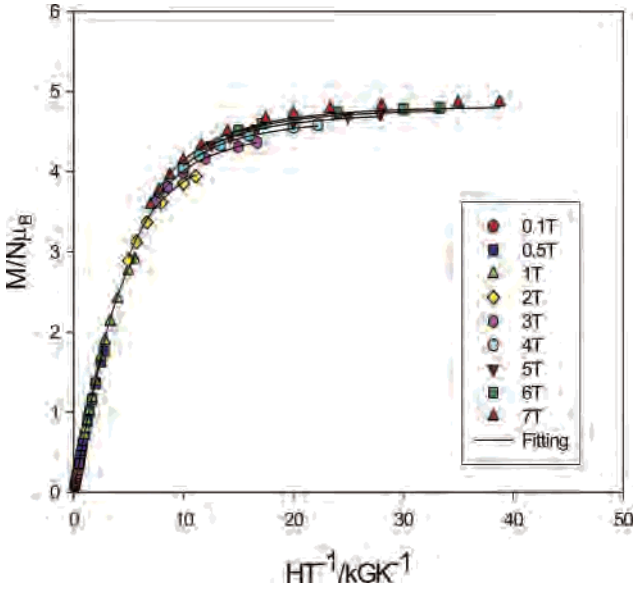

Figure 4. Plot of reduced magnetization ($M/N\mu_B$) vs H/T for complex **1**. The solid lines are the fit of the data; see the text for the fit parameters.

species, but we have occasionally found that the exact nuclearity and structure of the product is sensitive to the identity of the carboxylate employed. An example of this is the reaction of $[Fe_3O(O_2CR)_6L_3]^+$ species with dmemH.[44,45] Thus, we have also studied the product of reactions with hmbpH as a function of the carboxylate, but in this case have found that we obtain the same structural type in each case. Thus, the reaction of $[Fe_3O(O_2CR)_6(H_2O)_3]^+$ (R = Ph, Me, Bu^t)with 1−3 equiv of hmbpH in MeCN led to the isolation of the corresponding hexanuclear cluster $[Fe_6O_2(OH)_2(O_2CR)_6(hmbp)_4]^{2+}$ (R = Ph (**2**), Me (**3**), Bu^t (**4**)). The formation of this family is summarized in eq 2.

$$2[Fe_3O(O_2CR)_6(H_2O)_3]^+ + 4hmbpH \rightarrow [Fe_6O_2(OH)_2(O_2CR)_6(hmbp)_4]^{2+} + 6RCO_2H + 4H_2O \quad (2)$$

Description of Structures. A labeled representation and stereoview of complex **1** are shown in Figure 1. Selected interatomic distances and angles are listed in Table 2. Complex **1** crystallizes in monoclinic space group $P2_1/c$. The core can be described as consisting of a $[Fe_4(\mu_3\text{-}O)_2]^{8+}$ butterflylike subunit (Fe1, Fe3, Fe4, and Fe5), on the top of which is attached a $[Fe(\mu\text{-}OH)(\mu\text{-}OR)_3]$ unit containing Fe2. There is an O atom monoatomically bridging Fe2 to each of the four Fe atoms of the butterfly. Three of these O atoms (O3, O5, O6) are the alkoxide arms of the three hmbp$^-$ groups, and the fourth is the OH$^-$ ion (O4). The protonated OH$^-$ nature of O4 was confirmed by bond valence sum (BVS) calculations,[46] which gave a value of 1.09. The bipyridyl portions of two hmbp$^-$ groups chelate one each to the two wingtip Fe atoms, Fe1 and Fe3, while the third chelates Fe2. Peripheral ligation about the core is then completed by five acetate groups in the common $\eta^1{:}\eta^1{:}\mu$-bridging mode. It is interesting to note that bpy itself will react with Fe(III) in the presence of carboxylate groups to give the Fe_4 butterfly complexes of formula $[Fe_4O_2(O_2CR)_7(bpy)_2]^+$ with the two bpy groups attached at the wingtip Fe atoms.[17] Thus, the bpy 'fragments' of the hmbp$^-$ chelates are giving the analogous Fe_4 butterfly unit, but the alkoxide arms also then foster attachment of the fifth Fe atom. The core of complex **1** is unprecedented in pentanuclear iron(III) chemistry. Indeed, there are relatively few pentanuclear iron(III) complexes in the literature, and these have Fe_5 topologies such as a square pyramid, a centered tetrahedron, and a partial cubane extended at one face by a partial admantane unit.[47−56]

A labeled representation and stereoview of complex **2** are shown in Figure 2, and selected interatomic distances and angles are listed in Table 3. Complex **2** crystallizes in triclinic space group $P\bar{1}$. The core can be described as a modification of the structure of **1** and consists of a central $[Fe_4(\mu_3\text{-}O)_2]^{8+}$ flattened-butterfly unit (Fe2, Fe2′, Fe3, and Fe3′) on either side of which is attached a $[Fe(\mu\text{-}OH)(\mu\text{-}OR)_2]$ unit contain-

(44) Bagai, R.; Datta, S.; Bentacur-Rodriguez, A.; Abboud, K. A.; Hill, S.; Christou, G. *Inorg. Chem.* **2007**, *46*, 4535−4547.
(45) Laye, R. H.; Wei, Q.; Mason, P. V.; Shanmugam, M.; Teat, S. J.; Brechin, E. K.; Collison, D.; McInnes, E. J. L. *J. Am. Chem. Soc.* **2006**, *128*, 9020−9021.
(46) Brown, I. D.; Altermatt, D. *Acta Crystallogr., Sect. B: Struct. Sci.* **1985**, *B41*, 244−247.
(47) Tabernor, J.; Jones, L. F.; Heath, S. L.; Muryn, C.; Aromi, G.; Ribas, J.; Brechin, E. K.; Collison, D. *Dalton Trans.* **2004**, 975−976.
(48) Boskovic, C.; Sieber, A.; Chaboussant, G.; Guedel, H. U.; Ensling, J.; Wernsdorfer, W.; Neels, A.; Labat, G.; Stoeckli-Evans, H.; Janssen, S. *Inorg. Chem.* **2004**, *43*, 5053−5068.
(49) Boskovic, C.; Labat, G.; Neels, A.; Gudel, H. U. *Dalton Trans.* **2003**, 3671−3672.
(50) Lachicotte, R. J.; Hagen, K. S. *Inorg. Chim. Acta* **1997**, *263*, 407−414.
(51) Reynolds, R. A.; Coucouvanis, D. *Inorg. Chem.* **1998**, *37*, 170−171.
(52) O'Keefe, B. J.; Monnier, S. M.; Hillmyer, M. A.; Tolman, W. B. *J. Am. Chem. Soc.* **2001**, *123*, 339−340.
(53) Mikuriya, M.; Nakadera, K. *Chem. Lett.* **1995**, *3*, 213−214.
(54) Mikuriya, M.; Hashimoto, Y.; Nakashima, S. *Chem. Commun.* **1996**, 295−296.
(55) Herold, S.; Lippard, S. J. *Inorg. Chem.* **1997**, *36*, 50−58.
(56) Krishnamurthy, D.; Sarjeant, A. N.; Goldberg, D. P.; Caneschi, A.; Totti, F.; Zakharov, L. N.; Rheingold, A. L. *Chem. Eur. J.* **2005**, *11*, 7328−7341.

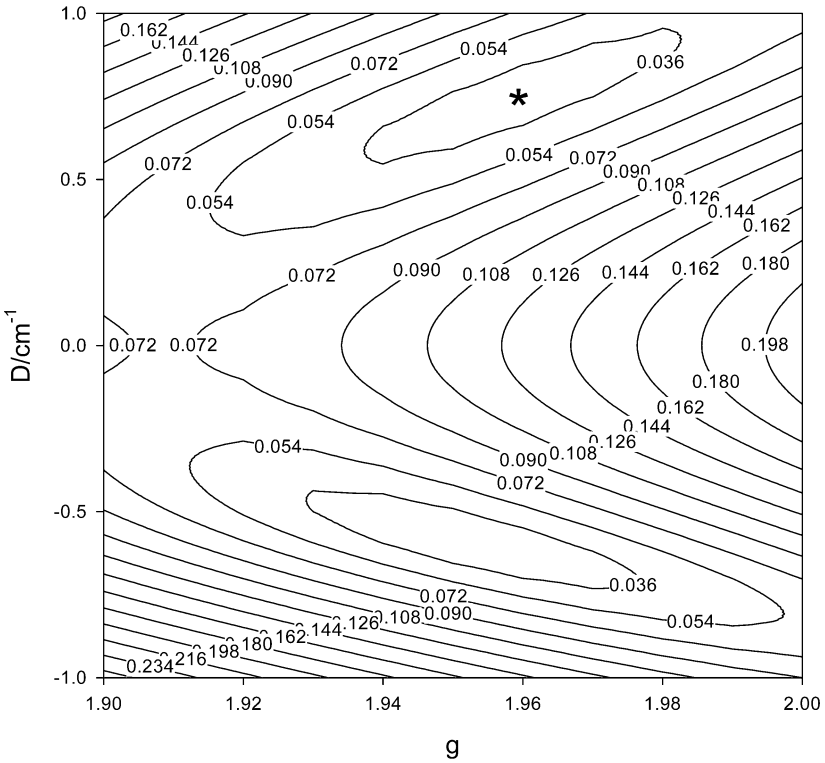

Figure 5. Two-dimensional contour plot of the fitting error surface vs D and g for **1**.

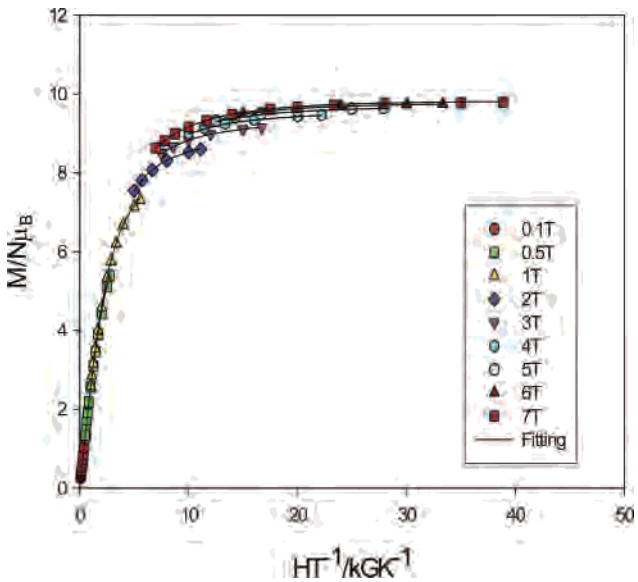

Figure 6. Plot of reduced magnetization ($M/N\mu_B$) vs H/T for complex **2**·H_2O. The solid lines are the fit of the data; see the text for the fit parameters.

ing Fe1 and Fe1′. There are now four hmbp$^-$ groups, two again on the wingtip positions of the butterfly unit, and one each on Fe1 and Fe1′. Unlike **1**, there are now only three monoatomically bridging O atoms linking Fe1 to the butterfly unit, two hmbp$^-$ alkoxide arms (O3′, O9) and the OH$^-$ group (O7). The OH$^-$ nature of O7 was again confirmed by BVS calculations, which gave a value of 1.16. The peripheral ligation about the $[Fe_6O_2(OH)_2(hmbp)_4]^{8+}$ core is completed by six benzoate groups, four in the η^1:η^1:μ-bridging mode and two in an η^1-terminal mode. The main overall difference between the core structures of **1** and **2** is that one of the wingtip hmbp$^-$ groups of **1** has rotated by 180°, bringing its alkoxide arm to the opposite side of the molecule from the fifth Fe atom and thus allowing attachment of a sixth Fe atom.

A number of other Fe_6 complexes have been reported in the literature, and these possess a variety of metal topologies such as planar, twisted boat, chair, parallel triangles, octahedral, ladderlike, cyclic, etc.[29,32−34,57] However, the only previous compounds somewhat structurally similar to **2** are **3**,[61] **4**[62] and **5**.[44] In these compounds there is again a central $[Fe_4(\mu_3\text{-}O)_2]^{8+}$ core with an additional Fe atom on each side (as in **2**), but the precise means by which the latter are connected to the Fe_4 unit are different from the situation in **2**.

Magnetochemistry. Solid-state, variable-temperature DC magnetic susceptibility data in a 0.1 T field and in the 5.0−300 K range were collected on powdered crystalline samples of **1**−**4** restrained in eicosane. The obtained data are plotted as $\chi_M T$ vs T in Figure 3. For **1**, $\chi_M T$ steadily decreases from 6.69 cm^3 mol^{-1} K at 300 K to 4.01 cm^3 mol^{-1} K at 5.0 K.

(57) Hegetschweiler, K.; Schmalle, H.; Streit, H. M.; Schneider, W. *Inorg. Chem.* **1990**, *29*, 3625−3627.
(58) Canada-Vilalta, C.; Rumberger, E.; Brechin, E. K.; Wernsdorfer, W.; Folting, K.; Davidson, E. R.; Hendrickson, D. N.; Christou, G. *J. Chem. Soc. Dalton Trans.* **2002**, 4005−4010.
(59) Shweky, I.; Pence, L. E.; Papaefthymiou, G. C.; Sessoli, R.; Yun, J. W.; Bino, A.; Lippard, S. J. *J. Am. Chem. Soc.* **1997**, *119*, 1037−1042.
(60) Grant, C. M.; Knapp, M. J.; Streib, W. E.; Huffman, J. C.; Hendrickson, D. N.; Christou, G. *Inorg. Chem.* **1998**, *37*, 6065−6070.
(61) Nair, V. S.; Hagen, K. S. *Inorg. Chem.* **1992**, *31*, 4048−4050.
(62) Ammala, P. S.; Batten, S. R.; Cashion, J. D.; Kepert, C. M.; Moubaraki, B.; Murray, K. S.; Spiccia, L.; West, B. O. *Inorg. Chim. Acta* **2002**, *331*, 90−97.

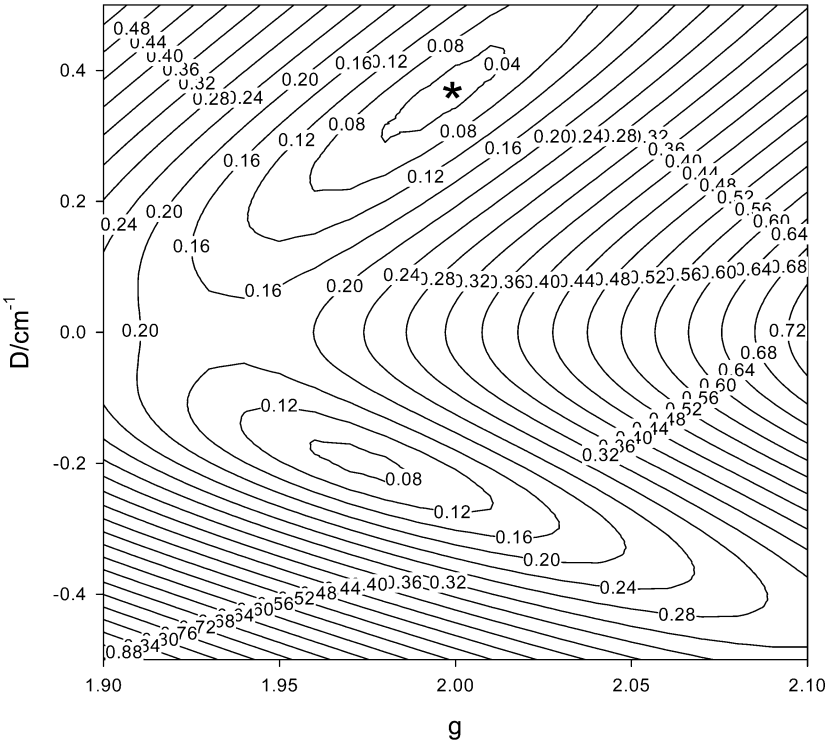

Figure 7. Two-dimensional contour plot of the fitting error surface vs D and g for **2**·H_2O.

The 300 K value is much less than the spin-only ($g = 2$) value of 21.87 $cm^3\ mol^{-1}$ K for five noninteracting Fe(III) ions, indicating the presence of strong antiferromagnetic interactions, as expected for oxo-bridged Fe(III) systems. The 5.0 K value of 4.01 $cm^3\ mol^{-1}$ K suggests a spin $S = 5/2$ ground state.

The $\chi_M T$ vs T plots for the three complexes **2**−**4** in Figure 3 are very similar, indicating a minimal influence of the different carboxylate groups and supporting the conclusion that not just their formulations are identical but also their structures. For this reason, we will give further details for representative complex **2**, for which the crystal structure is available. $\chi_M T$ for **2**·H_2O increases from 11.88 $cm^3\ mol^{-1}$ K at 300 K to a maximum of 14.9 $cm^3\ mol^{-1}$ K at 30 K, and then decreases very slightly to 14.65 $cm^3\ mol^{-1}$ K at 5.0 K. The $\chi_M T$ at 300 K is again much less than the spin-only value of 26.25 $cm^3\ mol^{-1}$ K expected for six noninteracting Fe(III) ions indicating the presence of strong antiferromagnetic interactions. However, the increase in $\chi_M T$ with decreasing temperature suggests that the lowest lying spin states are of high spin values, and the near-plateau value of 14.6−14.9 $cm^3\ mol^{-1}$ K at low temperatures is very close to the spin-only value of 15.0 $cm^3\ mol^{-1}$ K for an $S = 5$ ground state. The small decrease in $\chi_M T$ at the lowest temperatures is very likely due to the ZFS within the $S = 5$ ground state and perhaps some weak intermolecular interactions. The differences in $\chi_M T$ vs T for the three complexes are almost certainly just reflecting small differences in g values, intramolecular exchange coupling constants (J), ZFS parameters (D), and intermolecular antiferromagnetic interactions, but the overall almost identical $\chi_M T$ vs T plots indicates these factors are nevertheless almost identical for **2**−**4**.

To confirm the above ground state spin estimates, variable-field (H) and -temperature magnetization (M) data were collected in the 0.1−7.0 T and 1.8−10 K ranges. The resulting data for **1** are plotted in Figure 4 as reduced magnetization ($M/N\mu_B$) vs H/T, where N is Avogadro's number and μ_B is the Bohr magneton. The saturation value at the highest fields and lowest temperatures is ∼4.86, as expected for an $S = 5/2$ ground state and g slightly less than 2; the saturation value should be gS in the absence of complications from low-lying excited states. The data were fit, using the program Magnet,[63] by diagonalization of the spin Hamiltonian matrix assuming only the ground state is populated, incorporating axial anisotropy ($D\hat{S}_z^2$) and Zeeman terms, and employing a full powder average. The corresponding spin Hamiltonian is given by eq 3, where $\hat{S}_z$ is the easy-axis spin operator, g is the electronic g factor, μ_0 is the vacuum permeability, and H is the applied field. The last term in eq 3 is the Zeeman energy associated with an applied magnetic field.

$$\mathscr{H} = D\hat{S}_z^2 + g\mu_B\mu_0\hat{S}\cdot H \qquad (3)$$

The best fit for **1** is shown as the solid lines in Figure 4 and was obtained with $S = 5/2$ and either of the two sets of parameters: $g = 1.96$ and $D = 0.75\ cm^{-1}$, or $g = 1.95$ and $D = -0.59\ cm^{-1}$. Alternative fits with $S = 3/2$ or 7/2 were rejected because they gave unreasonable values of g and D. It is common to obtain two acceptable fits of magnetization data for a given S value, one with $D > 0$ and the other with $D < 0$, since magnetization fits are not very sensitive to the

(63) Davidson, E. R. *MAGNET*; Indiana University: Bloomington, IN.

Scheme 3

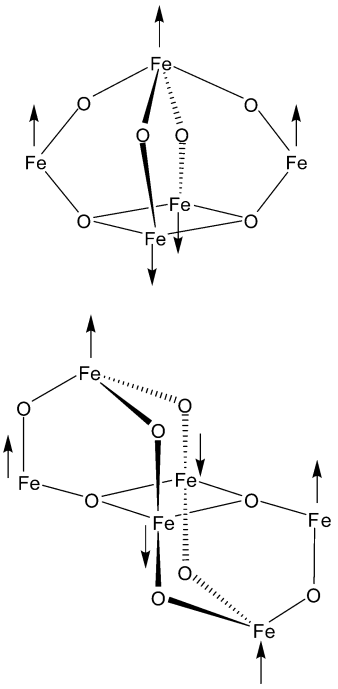

sign of *D*. This was indeed the case for the magnetization fits for all complexes **1**−**4** in this work. In order to assess which is the superior fit in all these cases and also to ensure that the true global minimum had been located for each compound, we calculated the root-mean-square error surface for the fits as a function of *D* and *g*. We show those for **1** and **2**·H_2O as two-dimensional contour plots below, and the rest are available as Supporting Information. For **1,** the error surface (Figure 5) clearly shows only two minima with positive and negative *D* values, with both fits being of comparable quality.

The reduced magnetization plots saturate at 9.78 for **2**·H_2O, 9.64 for **3**·H_2O, and 9.88 for **4**·H_2O, suggesting an $S = 5$ ground state and $g < 2$. The best fit for **2**·H_2O is shown as the solid lines in Figure 6, and was obtained with $S = 5$ and either $g = 2.00$ and $D = 0.36$ cm^{-1} or $g = 1.97$ and $D = -0.20$ cm^{-1}. In this case, the fit error surface (Figure 7) clearly shows that the fit with positive *D* is far superior, suggesting that this is the true sign of *D*. The best fit for **3**·H_2O was obtained with $S = 5$ and either $g = 1.98$ and $D = 0.46$ cm^{-1} or $g = 1.94$ and $D = -0.21$ cm^{-1}. For **4**·H_2O, the best fit was with $S = 5$ and either $g = 2.02$ and $D = 0.36$ cm^{-1} or $g = 1.99$ and $D = -0.19$ cm^{-1}. The corresponding figures and the two-dimensional *D* vs *g* error plots are available in Supporting Information, and they again show that the fits with positive *D* are the superior ones.

It is interesting to try to rationalize the observed ground state spin values of **1** and **2**. It is assumed that all Fe_2 pairwise exchange interactions are antiferromagnetic, as is essentially always the case for high-spin Fe(III), and there will thus be competing antiferromagnetic exchange interactions and spin frustration effects within the many Fe_3 triangular units in these complexes. The ground state of **1** is the easiest to rationalize: the discrete Fe_4 butterfly (rhombus) topology is known to usually give an $S = 0$ ground state as a result of the antiferromagnetic interactions along the four outer (wingtip−body) edges overcoming, and thus frustrating, the diagonal (body−body) interaction.[17,30,64−67] The structure of **1** comprises such an Fe_4 unit with an additional Fe above it, and assuming the same spin alignments as in the discrete Fe_4 molecules, then the ground state spin alignments are predicted to be those shown in Scheme 3 (top), giving the $S = 5/2$ ground state observed experimentally. Note that whether the spin of the fifth Fe atom is aligned parallel to the wingtip spins (as shown) or parallel to the body spins, an $S = 5/2$ ground state will still result as long as the interactions within the butterfly are stronger than those between it and the fifth Fe atom. This seems reasonable given that the interactions within the butterfly involve monoatomically bridging oxide ions. For **2**, we can again rationalize the ground state, using a simple extension of the argument for **1**, on the basis of a central $S = 0$ planar-butterfly unit coupling with the fifth and sixth Fe atoms as shown in Scheme 3 (bottom). This will give an overall $S = 5$ ground state for **2** as observed experimentally. It should be noted that we have sought to rationalize the ground states of **1** and **2** on the basis of previous observations for the Fe4 butterfly units and with as straightforward a description as possible. Thus, we have not invoked intermediate spin alignments of individual spins. In reality, the spin alignments leading to the observed $S = 5/2$ and 5 ground states could be more complicated than shown in Scheme 3.

None of the compounds exhibited an out-of-phase AC magnetic susceptibility signal down to 1.8 K in an AC field of 3.5 Oe oscillating with frequencies up to 997 Hz, indicating that they do not exhibit a barrier large enough vs *kT*, down to 1.8 K at least, to exhibit slow relaxation of their magnetization vectors, i.e., they are not single-molecule magnets. This is not surprising that the *D* values for **2**−**4** were concluded to be positive, whereas negative *D* values are required to yield the easy-axis (Ising) anisotropy necessary for SMMs. For **1**, we could not conclude the sign of *D*: assuming it is negative, the combination of $S = 5/2$ and $D = -0.59$ cm^{-1} would yield an upper limit to the magnetization relaxation barrier (*U*) of $U = (S^2-1/4)|D| = 3.5$ cm^{-1} $= 5.1$ K. Remembering that the actual or effective barrier (U_{eff}) is significantly less than *U*, it is not surprising that even with a negative *D* complex **1** does not display slow relaxation down to 1.8 K. Studies at much lower temperatures would be required to search for what would at best be a tiny barrier.

Conclusions

We have reported the initial use of a new N,N,O-based tridentate chelate in coordination chemistry, one that amal-

(64) Boudalis, A. K.; Tangoulis, V.; Raptopoulou, C. P.; Terzis, A.; Tuchagues, J. P.; Perlepes, S. P. *Inorg. Chim. Acta* **2004**, *357*, 1345−1354.
(65) Overgaard, J.; Hibbs, D. E.; Rentschler, E.; Timco, G. A.; Larsen, F. K. *Inorg. Chem.* **2003**, *42*, 7593−7601.
(66) Boudalis, A. K.; Lalioti, N.; Spyroulias, G. A.; Raptopoulou, C. P.; Terzis, A.; Bousseksou, A.; Tangoulis, V.; Tuchagues, J. P.; Perlepes, S. P. *Inorg. Chem.* **2002**, *41*, 6474−6487.
(67) Chaudhuri, P.; Rentschler, E.; Birkelbach, F.; Krebs, C.; Bill, E.; Weyhermuller, T.; Florke, U. *Eur. J. Inorg. Chem.* **2003**, *3*, 541−555.

gamates the chelating property of bpy with the chelating/bridging properties of the anion of hmpH. The resulting $hmbp^-$ has been employed in Fe(III) chemistry, and it has provided clean access to four new polynuclear Fe(III) clusters, **1**−**4**. The structures of **2**−**4** are concluded to be the same, given their identical formulation and almost superimposable magnetic properties. Note that identical formulation by itself does not mean identical structure: we recently reported two compounds, $[Fe_7O_4(O_2CPh)_{11}(dmem)_2]$ and $[Fe_7O_4(O_2CMe)_{11}(dmem)_2]$, that have the same formula (except for the carboxylate) but very different structures.[44]

The structures of **1** and **2** show the manifestation of the 'hybrid' bpy/hmp^- nature of $hmbp^-$ in that the bpy portion gives an Fe_4 butterfly subunit, as does bpy itself, while the alkoxide arm acts as an additional bridging group and raises the nuclearity to five or six. As a result, the complexes have significant ground state spin values of $S = 5/2$ and 5, respectively. It will be interesting to determine, as this work is extended, to what extent $hmbp^-$ will continue to provide a route to new metal clusters and to what extent these are related to clusters provided by bpy and hmp^- alone. Preliminary results employing $hmbp^-$ in Mn chemistry will be reported in due course.

Acknowledgment. We thank the National Science Foundation for support of this work.

Supporting Information Available: X-ray crystallographic data in CIF format for complexes **1**·5MeCN and **2**·3MeCN·H_2O, plots of $M/N_{\mu B}$ vs H/T, and two-dimensional contour plots of the fitting error surfaces vs D and g for **3**·H_2O and **4**·H_2O. This material is available free of charge via the Internet at http://pubs.acs.org.

IC070174I